WCEJ

WORLD CHEMICAL ENGINEERING JOURNAL

Journal homepage: http://jurnal.untirta.ac.id/index.php/WCEJ

# Simulation a Couple of Exothermic and Endothermic Syngas Processes in a Catalytic Plate Reactor

Masoud Safari[1*], Jafar Towfighi[1], Mohammad Torkian[1]

[1]*Department of Chemical Engineering, Tarbiat Modares University, Tehran, Iran*

*Corresponding Author Email: masoud.safari@modares.ac.ir

*ARTICLE HISTORY*

Received 24 March 2022
Received in revised form 10 May 2022
Accepted 14 May 2022
Available online 25 June 2022

*ABSTRACT*

This paper studies an efficient way to produce syngas from the methane couple reforming and partial methane oxidation by utilizing a catalytic plate reactor. Methane steam and dry reforming as endothermic reactions are coupled with partial methane oxidation as an exothermic reaction in a catalytic plate reactor, which is simulated using detailed reaction kinetics, mass, and energy balances. The impact of inlet temperature, composition, and velocities on the reforming and partial oxidation channels, and also the resulting methane conversions, is studied. In addition, the $H_2/CO$ ratio is evaluated for both endothermic and exothermic sides across varied feed ratios. Co- and counter-flow arrangements are simulated for catalytic plate reactors, and their impact on temperature distribution and methane conversion is studied. The suitable plate dimensions, in particular, plate length, are computed during this simulation. Applying a metal plate, Co- and counter-flow arrangements are simulated for catalytic plate reactors, and their impact on temperature distribution and methane conversion is studied. During this simulation, the appropriate plate dimensions, particularly plate length, are determined. The use of a metal plate with a greater thermal conductivity allows for effective heat transmission between endothermic and exothermic channels, resulting in outstanding temperature distribution and slight temperature differences.

**Keywords:** *Methane steam and dry reforming, catalytic plate reactor, partial oxidation of methane*

## 1. INTRODUCTION

While numerous technologies exist for the production of syngas [1-3] and other chemical products, there is an overriding need to achieve an efficient catalytic process in order to minimize energy usage. Reactors are the core of the chemical industry, as downstream processes are highly dependent on reactor performance, notably the degree of control, selectivity, and heat and mass transfer, all of which are highly interrelated. Additionally, upstream operations can be considered as phases whose primary aim is to prepare the reactants for input into the reactor. As a result, the reaction step has received greater attention in Process Intensification than other unit actions. Several enhanced reactors, either on the market or in development, attest to this. Several reactors are employed in gas synthesis processes, notably those that include solid heterogeneous catalysts in the form of stationary or moving particles of varying shapes and sizes. Steam reforming of natural gas, which is frequently employed to produce synthesis gas, is a highly endothermic process. The typical tubular reactors are employed, which are housed within the massive gas-fired furnaces. Significant amount of energy is consumed to raise the reaction temperature to the desired level by radiation from the flue gas and furnace walls. There are a variety of constraints and disadvantages associated with these traditional reactors, including increasing energy consumption, mass and heat transfer limitations, the low specific surface area of the catalyst, high pressure drops and thermal instabilities (runaway) in stationary beds, or catalyst attrition and device erosion in slurry reactors [4]. Researches has consistently demonstrated that these limits can be overcome by utilizing thin film catalysts, which are used in catalytic plate reactor technology. In comparison to conventional packed bed, slurry, or tubular reactors, the catalytic plate reactor generates

significant profits. It was first proposed by Hunter and McGuire [2], and it has been noted by Ramshaw and Anxionnaz et al. [6, 7].

Catalytic Plate Reactors (CPRs) contain nearby catalytically coated thin metal plates with crisscrossing channels or grooves. Exothermic and endothermic processes occur in opposite directions. The reduced size of the channel gap (order of millimeters) and catalyst layer (order of micrometers) minimizes the heat and mass transfer resistances leading to enhanced performance of this reactor type compared to conventional ones. Heat transfer is by conduction from the exothermic to the endothermic region. Potential applications for CPRs are in the coupling of strongly endothermic processes such as steam reforming, hydrocarbon dehydrogenation, or catalytic cracking, with an exothermic process, usually catalytic combustion [8]. This implication, coupling an exothermic and endothermic reaction on opposite sides of a plate forming part of a heat exchanger, significantly reduces size process intensification. The principal benefit of channel reactor technology is that thin catalyst films have much less resistance to transport processes than traditional catalyst pellets. Hence catalyst effectiveness factors would be near unity. Utilizing the catalyst as a thin layer (<50 μm) coated on the channel surface include excellent heat transfer characteristics by reducing heat transfer restrictions and minimal intra catalyst diffusion resistance in comparison with pellet catalysts and can enhance the effectiveness factor [9-11]. These profits lead to reactors that are smaller in size, with lower pressure drops than traditional alternatives. The smaller channel gap (order of millimeters) and catalyst layer (order of micrometers) reduce heat and mass transfer resistances, resulting in an increase in performance when compared to conventional reactors. Conduction is used to transmit heat from an exothermic to an endothermic zone. CPRs may be used to couple highly endothermic processes such as steam reforming, hydrocarbon dehydrogenation, or catalytic cracking with an exothermic process, most often catalytic combustion [8]. This implies that by linking exothermic and endothermic reactions on opposite sides of a plate consisting part of a heat exchanger, size process intensification is greatly reduced. The primary advantage of channel reactor technology is that thin catalyst films resist transport processes far better than standard catalyst pellets. As a result, the efficacy factors of the catalysts would be close to unity. In comparison to pellet catalysts, using the catalyst as a thin layer (50 m) coated on the channel surface provides superior heat transfer characteristics by eliminating heat transfer constraints and minimizing intra catalyst diffusion resistance, which can increase the efficacy factor [9-11]. These savings result in reactors that are smaller in size and have lower pressure drops than conventional reactors. Capital cost savings are substantial. Catalytic plate reactors can be used to accelerate a variety of industrial gas-phase reactions and promote in situ reforming of fuel feedstock for commercial fuel cell applications or the manufacture of syngas, which is used as a feedstock in a wide variety of industrial processes. The potential savings on capital costs are considerable. Catalytic plate reactors can intensify several industrial gas-phase reactions and promote in situ reforming of fuel feedstock for commercial fuel cell applications or the production of syngas, which is the feedstock for many industrial processes.

When conducting highly exothermic reactions in a fixed bed reactor, hotspots will emerge if the heat removal rates from the catalyst are insufficient. In comparison to conventional fixed bed reactors, thin catalyst coatings applied to heat transfer surface areas significantly increase the desirable products per unit volume yield in a CPR. CPR enhances the product spectrum of catalytic reactions that are extremely temperature dependent. Additionally, the performance of plate reactors is unaffected by scale differences. Scaling up CPR is accomplished by increasing the number of plates in the stack rather than by modifying the plate size. As a result, the time necessary for scaling up and modification from laboratory to commercial production is greatly decreased [12].

## 2. INTENSIFIED METHANE REFORMING (ENDOTHERMIC SIDE)

The principal syngas procedures for hydrogen production from methane are as follows: (1) Steam Reforming (SR), (2) Dry Reforming (DR), (3) Steam and Dry (Couple) Reforming (CR), (4) Autothermal Reforming (ATR), and (5) Partial Oxidation (POX). Three of the initial components undergo a very endothermic reaction, whereas POX undergoes an exothermic reaction. ATR is a mixture of SR and POX that has the advantage of being thermoneutral in operation. Although Steam and Dry (Couple) Reforming produces the highest hydrogen concentrations in comparison to ATR and POX [13], because to the reaction's extremely endothermic nature, the heat generated by the reaction should be given via an efficient technique. Figure 1 illustrates the three main procedures to produce syngas from methane that are included in this study. Catalytic methane combustion is an efficient method of supplying heat indirectly via a catalytic plate reactor (CPR). The three primary methods of methane reformation are as follows:

- Methane Steam reforming:

$$CH_4 + H_2O = CO + 3H_2 \qquad \Delta H = +206\ kJ/mol \qquad (1)$$

- Water Gas Shift:

$$CO + H_2O = CO_2 + H_2 \qquad \Delta H = -41\ kJ/mol \qquad (2)$$

- Methane Dry reforming:

$$CH_4 + 2CO_2 = 2CO + 2H_2 \qquad \Delta H = +247\ kJ/mol \qquad (3)$$

Steam reforming (SR) is the oldest and most practical method of converting $CH_4$ to $H_2$. It is a sequential parallel process that produces hydrogen and carbon dioxide ($CO_2$) by combining steam ($H_2O$) and fuel ($CH_4$) and reacting in a reformer in the presence of an active catalyst. Steam reforming methane (Reaction 1) creates

syngas with an $H_2/CO$ ratio greater than 3, which is then converted to water gas via the Water Gas Shift (Reaction 2). Ni and a few noble metals are the typical catalysts for SR [14-16]. This gas composition is suitable for operations that require a high concentration of hydrogen, such as $NH_3$ synthesis or iron ore reduction. Alternative syngas compositions can be obtained by carbon dioxide reforming methane; this process is referred to as dry reforming ($CO_2$ reforming) and results in an $H_2/CO$ ratio of 1 (Reaction 3) [17].

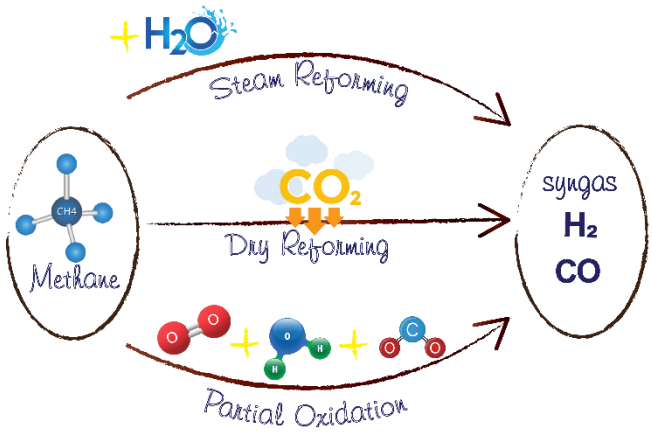


**Fig. 1**. Three main routes to produce syngas from methane

Dry reformation (DR) is a process in which two greenhouse gases, $CO_2$ and $CH_4$, are combined. In terms of environmental protection, methane DR can convert these two major greenhouse gases into syngas [18]. Although many natural gas resources contain some $CO_2$ and thus require less investment in the separation process, resulting in a much lower cost, there is a greater danger of carbon deposition on the catalyst pores under dry reforming settings as opposed to steam reforming conditions. Despite the fact that steam reforming has been widely industrialized as a means of producing synthesis gas with an $H_2/CO$ ratio greater than 3, it is an energy- and capital-intensive process [19].

Over last few decades, combined or mixed reforming of methane (CR) has garnered a significant amount of research from industrial and environmental perspectives [20-29]. The Fischer-Tropsch and methanol processes require a syngas ratio ($H_2/CO$) of at least two, and a variable syngas ratio can open up further industrial processes. As a result, this is an appropriate method for obtaining a diversified percentage of syngas in a single process, as it significantly reduces expenditure in setup and budgets for three different processes. By adding a suitable amount of oxidant, such as $H_2O$, to this process, the coke deposition problem in the system can be solved. [21, 30].

In order to adjust the syngas ratio ($H_2/CO$) by this process, the proportion among the reactants: $CH_4$, $CO_2$, and $H_2O$ should be manipulated according to the stoichiometry ratio of the reaction (4).

$$3CH_4 + CO_2 + 2H_2O = 4CO + 8H_2 \qquad (4)$$

The ordinary catalysts applied in coupled reforming of methane is Ni catalysts. Usually, Ni joints together with Ce, La, Co, Mg, and Mo [31-35].

The reaction rate equation utilized in this project was obtained from the literature [36-41]:

$$r_{11} = \frac{\frac{k_1}{p_{H_2}^{2.5}}\left(p_{CH_4}\cdot p_{H_2O} - \frac{p_{H_2}^3 \cdot p_{CO}}{K_{e,1}}\right)}{Den^2} \qquad \left[\frac{kmol}{kg_{cat}\cdot h}\right] \qquad (5)$$

$$r_{21} = \frac{\frac{k_2}{p_{H_2}^{2.5}}\left(p_{CO}\cdot p_{H_2O} - \frac{p_{H_2}\cdot p_{CO}}{K_{e,2}}\right)}{Den^2} \qquad \left[\frac{kmol}{kg_{cat}\cdot h}\right] \qquad (6)$$

Where

$$Den = 1 + K_{CO}\cdot p_{CO} + K_{H_2}\cdot p_{H_2} + K_{CH_4}\cdot p_{CH_4} - \frac{K_{H_2O}\cdot p_{H_2O}}{p_{H_2}} \qquad (7)$$

$$r_{31} = \frac{k_3\, K_{CH_{4\_2}}\, K_{CO_2}\left(\frac{p_{CH_4}\cdot p_{CO_2}}{p_{H_2}^{0.5}} - p_{H_2}^{1.5}\cdot p_{CO}\right)}{\left(1 + \frac{p_{CH_4}}{p_{H_2}^{0.5}\cdot K_{CH_{4\_2}}} + p_{CO_2}\cdot K_{CO_2}\right)^2} \left[\frac{kmol}{kg_{cat}\cdot h}\right] \qquad (8)$$

The values of pre-exponential factors and activation energies, with the correspondent dimensions, used in the Arrhenius expression, are presented as follow:

$$k_i = k_{i0}\cdot e^{\frac{-E_{ki}}{RT}} \qquad (9)$$

$$k_{10} = 1.1736\cdot 10^{12}, k_{20} = 54.3055\cdot 10^4, k_{30} = 3.59\cdot 10^{21} \qquad \left[\frac{kmol\cdot\sqrt{bar}}{kg_{cat}\cdot s}\right]$$

$$E_{k1} = 240.1, E_{k2} = 67.13, E_{k3} = 332.04 \qquad \left[\frac{kJ}{mol}\right]$$

The Van't Hoff equation relates the change in the adsorption constant, $K_{XY}$, of the chemical reactants to the change in temperature. So, the effect of temperature on the adsorption and retention behaviors of the compounds in catalysts can be considered. The value of pre-exponential factors and of the heats of adsorption used in the Van't Hoff expression are:

$$K_{XY} = K_{XY}^0\cdot e^{\frac{\Delta H_i}{RT}} \qquad (10)$$

$$K_{CH_4}^0 = 6.65*10^{-4}, K_{H_2O}^0 = 1.77*10^{+5}, K_{CO}^0 = 8.23*10^{-5}, K_{H_2}^0 = 6.12*10^{-9}, K_{CO_2}^0 = 3.53*10^{-8}, K_{CH_{4_2}}^0 = 2.89*10^{-8} \quad bar^{-1}$$

$$\Delta H_{CH_4} = -38.28, \Delta H_{H_2O} = 88.68, \Delta H_{H_2} = -82.9, \Delta H_{CO} = -70.65, \Delta H_{CO_2} = -125.39, \Delta H_{CH_{4_2}} = -109.68 \quad \left[\frac{kJ}{mol}\right]$$

And, equilibrium constants $K_{e,k}$ with k=1,2 are:

$$K_{e,1} = e^{\left(\frac{26830}{RT}+30.114\right)}, K_{e,2} = e^{\left(\frac{4400}{RT}-4.036\right)} \quad bar^2 \qquad (11)$$

## 3. PARTIAL OXIDATION (EXOTHERMIC SIDE)

It is well established that CR is an extremely endothermic reaction, whereas POX is an exothermic

reaction. If these two processes work well together, the heat energy generated by the POX reaction can be used to power the CR process.

The catalytic partial oxidation of methane to produce synthesis gas has received considerable interest in recent years [42]. Catalytic partial oxidation of methane is a cost-effective and technically feasible technology for synthesis gas production. Due to the process's modest exothermic nature and the lower $H_2$:CO ratio of around 2, it is less energy- and capital-intensive than downstream procedures such as methanol synthesis and Fischer-Tropsch synthesis of higher hydrocarbons. Additionally, a fuel processor based on this technique could provide a low-cost, compact system capable of rapid startup and load fluctuation, which is more suitable for fuel cell electric cars [43].

The partial oxidation of methane to synthesis gas can be accomplished in one of two ways. According to the indirect reaction scheme, a portion of methane is combustible to $CO_2$ and $H_2O$ via complete oxidation followed by reforming reactions in which the remaining methane reacts with $CO_2$ and $H_2O$ to produce CO and $H_2$ (16-18).

$$CH_4 + \frac{1}{2}O_2 = CO + 2H_2 \qquad \Delta H = -35\ kJ/mol \qquad (12)$$

$$CH_4 + 2O_2 = CO_2 + 2H_2O \qquad \Delta H = -801\ kJ/mol \qquad (13)$$

$$CH_4 + CO_2 = 2CO + 2H_2 \qquad \Delta H = +247\ kJ/mol \qquad (14)$$

$$CH_4 + H_2O = CO + 3H_2 \qquad \Delta H = +206\ kJ/mol \qquad (15)$$

The total partial oxidation reaction equation which our ratios of reactants extracted from it, is described as follow:

$$5CH_4 + 3O_2 = 9H_2 + 5CO + H_2O \qquad (16)$$

A variety of catalysts, including nickel, cobalt, and noble metals (Rh, Pt, Ru), have been adapted for the partial oxidation of methane [44-53]. The great majority of catalysts wish to operate at temperatures between 700 and 1000 K. Ni and Ru both serve as notable indirect scheme catalysts. Despite their high conversion and selectivity, Ni catalysts suffer from deactivation due to coke production. Cobalt-based catalysts are less active for syngas methanation than nickel-based catalysts. As a result, cobalt-based catalysts may represent an intriguing alternative to nickel-based catalysts [54,55]. The primary drawbacks of cobalt catalysts are their decreased activity and stability [48,49]. Although Ru catalysts exhibit excellent activity and stability, they are expensive and difficult to get. A significant number of indirect catalytic systems are based on $Ru/TiO_2$ [56].

The alternative is a direct conversion of methane to synthesis gas that does not involve the creation of $CO_2$ or $H_2O$ as chemical intermediates, as described in Eq. 12. It has been accomplished under specific conditions using methane and oxygen catalysts [57-59]. This is highly dependent on the oxygen availability on the catalyst surface and the strength of the oxygen-surface connection [57]. The issue with industrializing synthesis gas generation using this technique is the reactivity of oxygen with the principal products - carbon monoxide and hydrogen - which results in the formation of carbon dioxide and water [60]. This restricts the amount of synthesis gas that may be obtained from the direct reaction of methane and oxygen at lower temperatures. As a result, some attempts are being made to determine the optimal catalyst performance while avoiding significant mass and heat transfer concerns. Recent research indicates that oxygen in solid oxidized platinum has a high activity for oxidizing methane to syngas but a poor activity for oxidizing hydrogen and carbon monoxide [59]. Oxygen bonded or dissolved in a solid platinum matrix was shown to be less reactive than oxygen supplied in the gas phase, resulting in a significant increase in syngas selectivity. This finding was proposed to be related to the well-balanced ratio of oxygen diffusion rate in platinum to the residence times of reacting species on the surface, which adjusts the oxygen availability on the surfaces so that the reaction proceeds with stoichiometrically favorable amounts of syngas generation. However, platinum is a somewhat expensive material, and the enormous amounts required to produce an adequate oxygen reservoir preclude any development of practical catalysts using only platinum. Cerium and ceria-zirconia oxides have been demonstrated to have a high capacity for oxygen storage and acceptable release characteristics in a variety of applications [61-65].

To accurately model a chemical reaction, it is critical to obtain precise information about the kinetic properties of the catalyst used. Additionally, it encompasses the complex mass transfer and diffusion processes that occur between the gas phase and the catalyst surface, as well as within the catalyst itself. In brief, the following are the kinetic rate equations for the reactions in the indirect scheme investigated in this study [66]:

$$r_{CH_4} = \frac{k_4 k_5 K_0 P_{CH_4} P_{O_2}}{k_5 K_0 P_{O_2} + k_5 K_1 K_0 P_{O_2} P_{CO} + k_4 P_{CH_4} + k_4 K_0 P_{CH_4} P_{O_2}} \qquad (17)$$

$$r_{CO_2} = \frac{k_5 k_6 K_1 K_0 P_{CO} P_{O_2}}{Den2} \qquad (18)$$

$$r_{CO} = r_{CH_4} - r_{CO_2} \qquad (19)$$

$$r_{H_2O} = \frac{(8.25 * 10^{-5})\, k_5 K_0 {P_{H_2}}^{0.5} P_{O_2}}{Den2} \qquad (20)$$

$$r_{H_2} = 2r_{CH_4} - r_{H_2O} \qquad (21)$$

$$Den2 = (1 + K_0 P_{O_2})\left(k_5 K_0 P_{O_2} + k_5 K_1 K_0 P_{O_2} P_{CO} + k_4 P_{CH_4} + k_4 K_0 P_{CH_4} P_{O_2}\right) \qquad (22)$$

where $T_r$ = 973 K and $k_{i,T}$, $K_{j,T}$ the rate and equilibrium constants, respectively, of the corresponding elementary reactions at 973 K:

$$k_i = k_{i,T}\, exp\left[\frac{-E_i}{R}\left(\frac{1}{T} - \frac{1}{T_r}\right)\right] \qquad i = 4,5,6 \qquad (23)$$

$$K_j = K_{j,T}\, exp\left[\frac{-\Delta H_j}{R}\left(\frac{1}{T} - \frac{1}{T_r}\right)\right] \qquad j = 0,1 \qquad (24)$$

The pre-exponential factors $k_{i,T}$, $K_{j,T}$ were calculated from the $k_{i0}$, $K_{j0}$, and $E_i$ and $\Delta H_j$ values by the Arrhenius and van't Hoff equation and the predicted values of model parameters are shown in below [66]:

$$k_{i0} = k_{i,T}\, exp\left[\frac{E_i}{RT}\right] \qquad (25)$$

$$K_{j0} = K_{j,T}\, exp\left[\frac{\Delta H_j}{RT}\right] \qquad (26)$$

$$k_{40} = 9.5 * 10^{-4}\,[\frac{mol}{g * s * kPa}], \qquad k_{50} = 4.5 * 10^{8}\,[\frac{mol}{g * s}], \qquad k_{60} = 1.1 * 10^{3}\,[\frac{mol}{g * s}], \quad K_{00} = 9.6 * 10^{-12}\,[kPa^{-1}], \quad K_{10} = 1.4 * 10^{-10}\,[kPa^{-1}]$$

$$E_4 = 27, E_5 = 206, E_6 = 116, \Delta H_0 = -172, \Delta H_1 = -173 \quad \left[\frac{kJ}{mol}\right]$$

## 4. DESCRIPTION OF THE MODEL AND CPR STRUCTURE

The endothermic (methane reforming) and exothermic (partial methane oxidation) processes for producing syngas are modeled in this simulation using a catalytic plate reactor. The linked set of partial differential equations is solved using the simulation software tool COMSOLTM 5.5. COMSOLTM use the finite element method to simulate the linked set of heat, mass, and flow equations (FEM). CPR models are constructed on the basis of a distributed mapped mesh. At the catalyst inlets, where reaction rates and heat gradients are more variable, more mesh elements are utilized. All solutions are resolved using fine meshes, and convergence requirements of $1*10^{-5}$ absolute error are used for all runs. Figure 2 illustrates the two-dimensional representation of the CPR configurations studied in this work. A comprehensive two-dimensional model has been expanded to include a CPR and to assume that the process is carried out adiabatically.

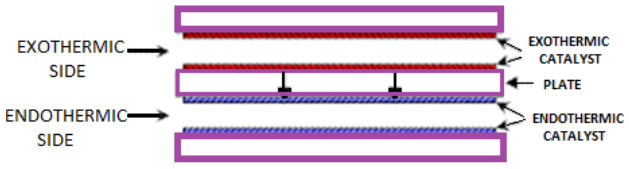


**Fig. 2.** 2D schematic of the simulated domains of the two endo- and exo-thermic syngas processes.

Three distinct domains can be distinguished: channel 1, which is used for endothermic reactions (Methane Reforming), channel 2, which is used for exothermic reactions (partial methane oxidation), and solid wall (Catalyst Layers). Ni supported on an alumina washcoat with the addition of Ba, Cr, Rh, and $La_2O_3$ is used as a catalyst layer for methane reforming reactions [41]. $RurTiO_2$ catalyst films are used in the partial methane oxidation reaction [66]. An aluminum plate separates the endothermic and exothermic catalyst layers. Despite the fact that the metallic plates support the catalyst layers, they must convey the effective heat flux between the exothermic and endothermic reaction zones. The model incorporates gas and solid phase heat and mass balances. Only within the catalyst layers do reactions occur, and hence the generation terms are absent from the mass balances of the species in the gas phase (channels). In the catalytic layers, on the other hand, convective momentum is absent, and only energy and mass balances are considered.

In order to model fluid flow through pores in a porous medium the Darcy's Law interface is applied. It can be used to simulate low velocity flows or media where the permeability and porosity are very small, and for which the pressure gradient is the main driving force and the flow is significantly impacted by the frictional resistance within the pores.

The assumptions for the modeling study are described in follow:

- Ideal gas law (high temperature and low pressure conditions).
- A double channel used to represent the entire reactor.
- Steady state is considered for reactor operation in a co-current flow arrangement.
- No thermal cracking and carbon formation reactions.
- All reactions take place in the catalyst layer.
- Catalyst layers were assumed thin adequate, so no intraphase diffusion limitations in the catalyst.
- Diffusive mass flux and conductive heat flux at reactor outlet are assumed to be zero.
- Heat transfer by radiation and pressure drop along reactor channels are negligible.
- Body forces are neglected.

According to the above assumption, for layers and channels the due momentum, energy and mass balances were employed together with the suitable limiting conditions as follow [39]:

**Gas Phase (Channels)**

➢ Material balances:

$$\rho_j u_{zj} \frac{\partial m_{i_j}}{\partial z} = \frac{\partial}{\partial x_j}\left(\rho_j D_{G_{in},j} \frac{\partial m_{i_j}}{\partial x_j}\right) + \frac{\partial}{\partial z}\left(\rho_j D_{G_{in},j} \frac{\partial m_{i_j}}{\partial z}\right) \quad (27)$$

➢ Energy Balances:

$$\rho_j u_{zj} C_{pj} \frac{\partial T_j}{\partial z} = \frac{\partial}{\partial x_j}\left(k_j \frac{\partial T_j}{\partial x_j}\right) + \frac{\partial}{\partial z}\left(k_j \frac{\partial T_j}{\partial z}\right) \quad (28)$$

➢ Boundary conditions:

1. Inlet conditions: $z = 0;\ \forall x_j$
   - inlet composition: $m_{i_j} = m_{i_j}^0$
   - inlet temperature: $T_j = T_j^0$
2. Outlet conditions: $\forall x_j;\ z = L$ zero flux: $\frac{\partial m_{i_j}}{\partial z} = \frac{\partial T_j}{\partial z} = \frac{\partial u_{zj}}{\partial z} = 0$
3. Symmetry Conditions at channel center: $\forall z;\ x_j = 0$ $\frac{\partial m_{i_j}}{\partial x_j} = \frac{\partial T_j}{\partial x_j} = \frac{\partial u_{zj}}{\partial x_j} = 0$

**Catalyst layers**

- Material balances:

$$\rho_j D_{effi,j} \frac{\partial m_{i_j}}{\partial x_j} = \vartheta_{ij}\ M_{ij}\left(r_{rj}\ + r_{rj} + r_{rj}\right) \quad (29)$$

- Energy Balances:

$$k_j \left[\frac{\partial T_j}{\partial x_j}\right]_{x_j=R_j} = r_{rj}\left(-\Delta H_{rj}\right) + r_{rj}\left(-\Delta H_{rj}\right) + r_{rj}\left(-\Delta H_{rj}\right) + \lambda_j \left[\frac{\partial T_s}{\partial x_s}\right]_{x_s} \quad (30)$$

$for\ j = 1{:}\ x_s = 0\ , for\ \ j = 2{:}\ x_s = \delta$

- Boundary conditions:

1. Inlet conditions: $z = 0;\ \forall x_s;\ \frac{\partial T_s}{\partial z} = 0$
2. Outlet conditions: $z = L;\ \forall x_s;\ \frac{\partial T_s}{\partial z} = 0$
3. Endothermic wall (channel, j=1): $\forall z;\ (T_s)_{x_S=0} = (T_1)_{x_1=R_1}$
4. Exothermic wall (channel, j=2): $\forall z;\ (T_s)_{x_S=\delta} = (T_2)_{x_2=R_2}$

Physical properties like as thermal conductivities and diffusion coefficients have been extracted and calculated from experimental values [36, 67] and the dependence of them to the values of component is evaluated via the following expressions:

Thermal conductivity: $k = k_0 \left(\frac{T}{T_0}\right)^{0.75}$ (31)

The diffusivity coefficients are computed for a binary mixture between component $i$ and $n = H_2O$ (the component present in excess at reforming channel) or ($i\ and\ n = CH_4\ at$ exothermic channel). The effective diffusion coefficient for the catalyst layer is [36, 67]:

$$D_{effin} = \frac{\varepsilon}{\tau}\left(\frac{1}{D_{k_{in}}} + \frac{1}{D_{G_{in}}}\right)^{-1} \quad (32)$$

Where $\varepsilon$ is the catalyst porosity, considered in the present evaluation to be 0.5, $\tau$ is the tortuosity that is equal to 4, $D_{k_{in}}$ and $D_{G_{in}}$ respectively the Knudsen diffusion coefficient and the molecular diffusion coefficient. Molecular diffusion coefficient is calculated using [36]:

$$D_{G_{in}} = \frac{0.1013\ .\ T^{1.75}\left(\frac{1}{M_i} + \frac{1}{M_n}\right)^{0.5}}{\pi[(\sum v_i)^{1/3} + (\sum v_n)^{1/3}]} \quad (33)$$

Where $\pi$ is the total pressure of the system, $M_i$ and $M_n$ are the molecular weights of species $i$ and n, and $v_n$is the atomic diffusion volume, characteristic for each component [36].

Knudsen diffusion coefficient is calculated using [36]:

$D_{k_{i,n}} = 97.\ R_p \sqrt{\frac{T_j^{cat}}{M_{i,j}}}$ (34) with $R_p$ the pore radius.

In order to set up a reference point, therefore the Effect of diverse parameters should be considered, calculations are first implemented for a "base case", for which base conditions are given as below:

- Inlet gas temperature, both endothermic and exothermic side: 850 K
- Inlet composition, reforming side: $CH_4$:1, $H_2O$:2, and $CO_2$: 0.667
- Inlet composition, exothermic side: $CH_4$:0.625, and $O_2$: 0.375
- Inlet velocity, endothermic side: 0.05 m/min and exothermic side: 0.01 m/min
- Inlet pressure, endothermic side: 1 bar and exothermic side: 1 bar
- Reactor dimensions and plate material features:
  - parallel plates of $20mm \times 40mm$
  - the height of channels: 3.6mm
  - catalyst layer thickness: 0.3mm
  - plate thickness: 1mm
  - plate material: Aluminum
  - plate thermal conductivity: 220 W/m$^2$ *K

## 5. RESULTS AND DISCUSSION

The findings of the CPR simulation are provided and compared on both sides in this section. The percent methane conversion and temperature profiles along the axial directions of the reforming and exothermic sides are compared, as well as the evolution of gas synthesis efficacy factors as a function of flow distribution. Additionally, the entrance gas velocity of the reactants and their compositions are compared in terms of percent conversion throughout the reforming and partial oxidation processes. Additionally, temperature profiles of endothermic and exothermic channels were recovered for a variety of plate materials with varying thermal conductivity. The performance of a reactor is determined using conversion, which is computed using the following equation:

$$X_j(z) = \left[\frac{\left(C_{0\_}CH_4\right)_j - \left(C\_CH_4\right)_j}{\left(C_{0\_}CH_4\right)_j}\right] * 100 \quad (36)$$

where $C_{0\_}CH_4$ is the initial concentration of the methane and $C\_CH_4$ is the local concentration of the methane that evaluated along the plate reactor.

### 5.1. Temperature distribution

Figure 3 shows the absorption and production of heat in the reforming and partial oxidation sides of the CPR, respectively. To find out how effective heat is distributed in the CPR, it is important to study the temperature profiles. The present model, that couples endothermic and exothermic catalytic reactions in the CPR, is clearly illustrated in this depict. Although both gases enter the CPR in the temperature of 850 K, in the exothermic side the partial oxidation occurs quickly and includes a considerable increase in temperature of gas to 867 K, the principal feature of this kind of reactor creates a balance between exothermic and endothermic channels by exchanging the heat through each other, as result the temperature of partial oxidation channel goes down to the inlet temperature, 850 K. As the chart shows, in order to absorb the heat along the plate in the endothermic channel, there is a slightly higher temperature in vicinity of divided plate in respect to all the its space which its distinction is 0.1 K roughly. This heat supporting from exothermic channel to endothermic side supply the essential heat for methane reforming reactions that are

noticeable endothermic reactions. Consequently, the suitable and adequate heat exchange in the reactor creates a moderate uniform temperature in all domines. So, it is possible to conduct the process in the lowest variable temperature conditions.

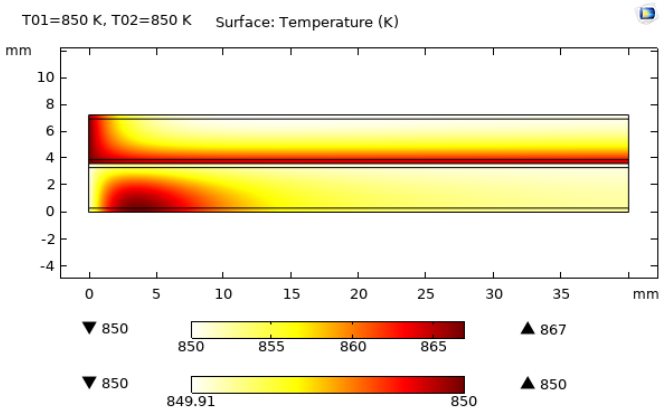


**Fig. 3.** Temperature profiles/Co-Current

## 5.2. Effect of Inlet Temperature

The figures 4 and 5 illustrate methane conversion at various inlet temperatures along the reactor's length for the reforming and partial oxidation channels, respectively. Across the whole reactor length, greater incoming gas temperatures result in higher CH4 conversions.

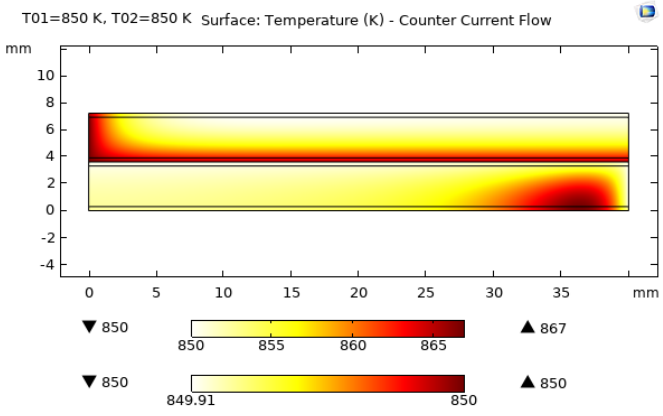


**Fig. 4.** Feed temperature in reforming channel

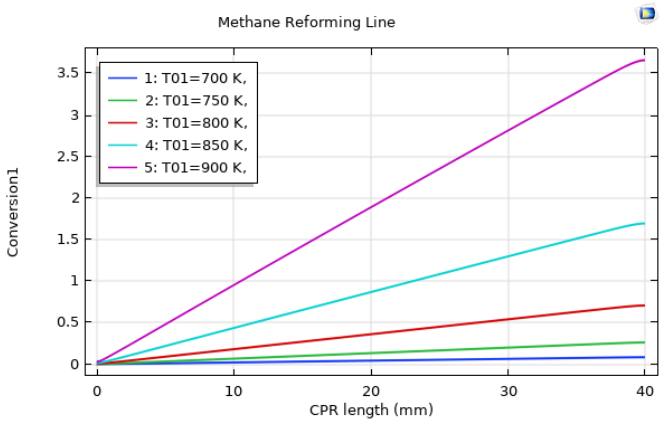


**Fig. 5**. Feed temperature in partial oxidation channel

Increased intake temperature leads in increased gas temperature throughout the cycle. This has an effect on both the catalyst activation and the activation of chemical processes. Despite the fact that increasing the inlet temperature favors endothermic reactions (steam and dry reforming), as illustrated in Figure 5, increasing the partial oxidation inlet gas temperature results in a considerable increase in methane conversion at 850 K. Additionally, at 900 K, 100% methane conversion is possible. In comparison, there is a slight fall in methane conversion that results in around 10% conversion along the length of the POX channel at 800 K, and no change in conversion below 750 K.

Similarly, a considerable increase of methane conversion can be acquired along the methane reforming channels by increasing the temperature. Although at the range of 700 to 800 K there is a slight rise trend and the acquired results are less than 1percent conversion, the dramatic growth of methane conversion can achieve since 850 K and the highest conversion in the reforming line gains at 900 K. The thermal results in these two parts are in consistence with the results of the literatures [39, 66, 68-69].

## 5.3. Effect of flow arrangement

In this section, the impact of flow arrangement on the heat transfer effects arising in the CPR from the exothermic partial oxidation reaction to the endothermic reforming reaction was studied. The most important issue in a CPR, is to examine how effective heat distribution is achieved throughout the reactor. Co-current and counter-current flow operation functions were simulated by considering the same initial conditions and kinetic model. Figures 3 and 6 present the temperature difference profile along the reactor length for the co-current and counter-current flow arrangements, respectively.

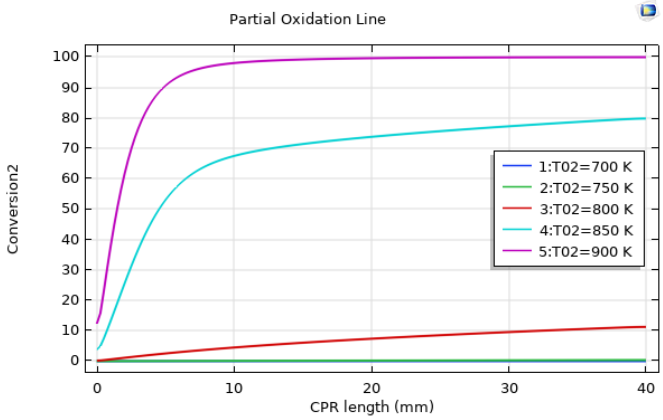


**Fig. 6.** Temperature profiles/Counter-Current

The plate temperature peaks near the inlet of the oxidation channel, since the feed gas of POX reacts instantly the temperature in the oxidation channel shoots up very close to the inlet. Although, generally co-current configuration can mitigate hot spot formation [70], according to literatures [68, 71] figures 7 and 8 for the

reforming and partial oxidation channels, respectively show that for the same conditions, counter-current configuration results in higher conversion compared to co-current arrangement in figures 4 and 5.

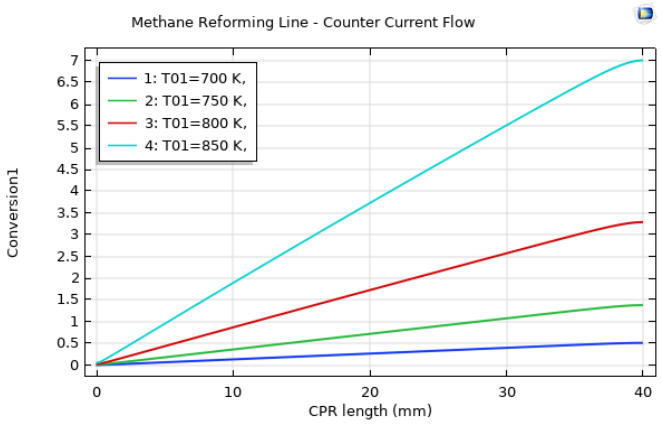


**Fig. 3.** Conversion in methane reforming channel/Counter

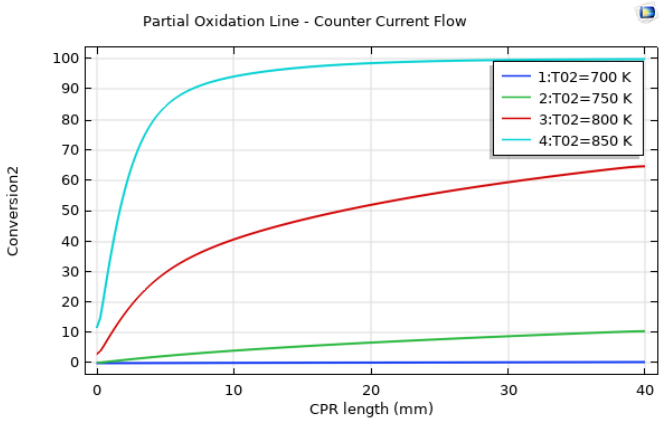


**Fig. 4.** Conversion in partial oxidation channel/Counter Current

In comparison methane conversion results from reforming channels which show in figures 7 and 4, a substantial growth in counter-current, approximately 5 times can be found out. The highest conversion in the reforming side of co-current arrangement at the temperature 900 K in the outlet position is around 3.5%. On the other hand, as the figure 7 demonstrates this amount of conversion can obtain at noticeable lower temperature, 800 K, and at the 850 K a sharp increase in methane conversion gains equal 7% in the counter-current pattern.

Furthermore, in partial oxidation channel exists a significant growth in counter-current configuration for methane conversion in contrast of co-current configuration. As the figure 8 illustrates, the perfect conversion in the counter-current arrangement can achieve at 850 K that depicts by blue line, in contrast this range of conversion in co-current arrangement exists at 900 K. Due to heat consumption reduces significantly in the counter-current pattern and the efficient applying energy intensifies growth of conversion through the length of plate reactor dramatically, in particular, in the reforming channel.

### 5.4. Effect of Feed Ratio

The reaction network in the reforming channel involves three inlet species; $CH_4$, $H_2O$, and $CO_2$ and in the POX channel includes two species; $CH_4$, and $O_2$. Comparison of the methane conversion and the ratio of syngas compositions by applying different inlet species compositions in the reforming and partial oxidation channels along the length of the reactor are illustrated in the figures 9-12 based on the initial conditions which they have adequate concordance with literatures results [66, 69, and 72].

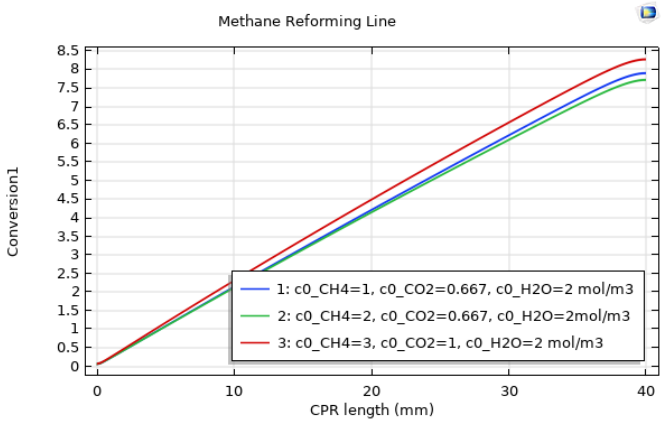


**Fig. 5.** Conversion in methane reforming channel/ Feed Ratio

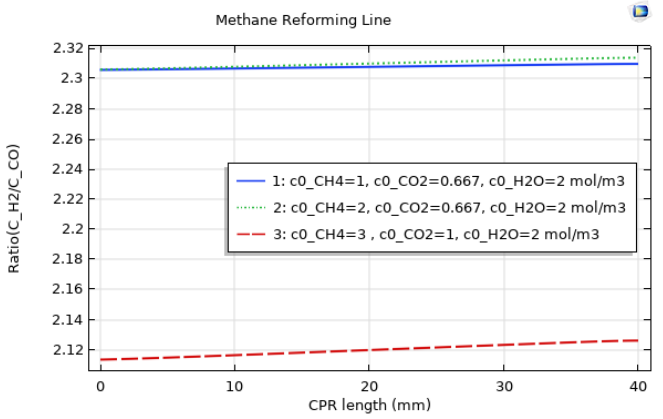


**Fig. 6.** Methane reforming channel/Ratio ($H_2$/CO)

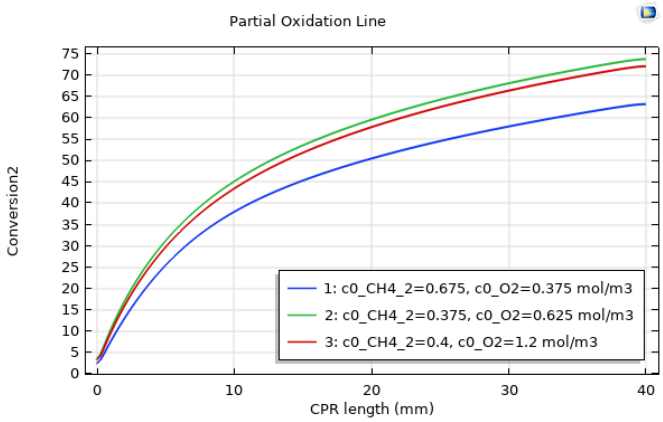


**Fig. 7.** Conversion in POX channel/Feed Ratio

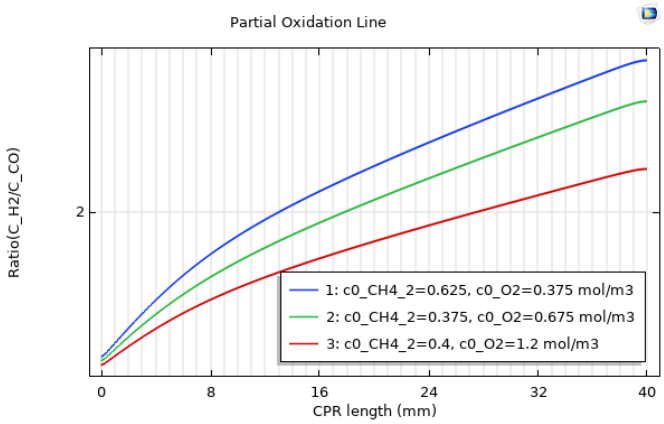


**Fig. 8.** POX channel/Ratio ($H_2$/CO)

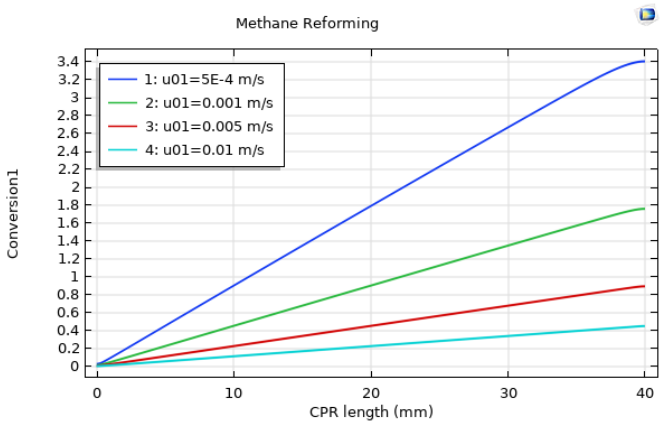


**Fig. 9.** Methane reforming/Feed Velocity

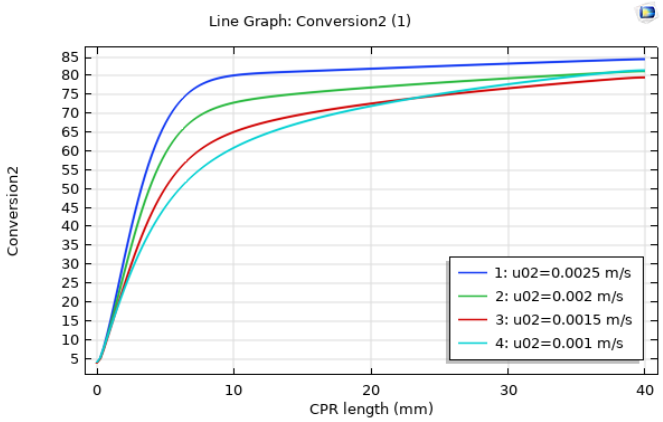


**Fig. 10.** POX/Feed Velocity

Regarding the methane reforming reaction equation (4), by utilizing the stochiometric ratio in feed ratio, ($CH_4/CO_2/H_2O$ =3/1/2), the most conversion trend along the length of reactor is extracted. Although this proportion has the highest conversion, it consumes the most methane. Moreover, as the figure 10 shows, due to this proportion the closest ratio of $H_2$/CO to 2 is achieved. According to the figure 9, the second trend with a moderate difference belong to our base simulation composition, $CH_4/CO_2/H_2O$ =1/0.667/2, which is extracted from [72]th reference. In comparison, despite the fact that this ratio has around less than 0.5% difference with the stochiometric ratio, it consumes just one third rate of $CH_4$ respect to the first ratio. Afterward, the lowest trend places with a tiny distinction from the base composition by this ratio $CH_4/CO_2/H_2O$ =2/0.667/2. Should the feed ratios compare in the efficiency of methane consumption rate, the third trend located at the second position. As the figure 10 illustrates, although the two last proportions have the best efficiency in methane consumption, they have the most ratio of $H_2$/CO around 2.31.

In contrast, as the figure 11 demonstrates, despite the stochiometric coefficient of reaction equation (16) as the feed ratio, $CH_4/O_2$=0.625/0.375=5/3, is applied in the partial oxidation channel, the lowest methane conversion among the three various ratios is acquired, near to 65%. However, according to the figure 12, this proportion creates the highest ratio of $H_2$/CO approximately 4. Should the stochiometric feed ratio reverse, the results change as opposed to the first trend and the highest conversion occurs. Furthermore, the ratio of $H_2$/CO declines in respect to the first feed ratio, roughly close to 3. In mathematical view due to reduction of the methane initial concentration, the dominator of conversion equation (36) will decrease and in follow the conversion amount will decline. In addition, in analytical view since in the excess of $O_2$ the oxidation equation (13) that is an instant reaction occurs dramatically and in the absence of adequate methane the consecutive reactions (14 and 15) will not happen. Hence, if the concentration of $CH_4$ is less than $O_2$, $CH_4$ will consume rapidly and although the methane conversion is growth, the rate of syngas production will reduce. As the figure 12 illustrates, this trend will intensify in the present of excessive $O_2$ that the $H_2$/CO goes down near to 2.5.

### 5.5. Effect of Feed Velocity

While reactor geometry, inlet operating conditions and catalyst loading are fixed, then variations of fluid velocities result in residence times. As figure 13 illustrates how the reactor behaves when velocities are raised since conversions are significantly decreased to around 0.4 for reforming. In order to achieve high conversions, one should decrease the inlet velocities. The highest conversion occurs at the lowest velocity 0.5mm/s and this pattern continues for the other velocities. Reforming reaction is an exothermic reaction so it is essential for the adequate progress of the reaction a sufficient residence time is supplied and it is happened only in the slight velocities.

Regarding the partial oxidation channels, as the figure 14 shows, although due to the oxidation is an instant reaction and it goes forward the vast majority of POX process rapidly, it is clear that velocity of inlet gas has not a significant Effect on the methane conversion. However, in the highest velocity the highest conversion occurs. As a result, the most conversion 85% take places at the highest velocity 2.5mm/s and the other velocities has the same consequence around 80% conversion. In both depicts, there is an appropriate conformity to the literatures results [68, 70].

### 5.6. Effect of Plate Thermal Conductivity

The thermal conductivity of the wall is an important design parameter, since it impacts heat exchange between channels as well as along the reactor. Figures 15 and 16 present channel centerline temperature profiles along the reactor for both sides meanwhile applying four metallic wall types with various thermal conductivity. They are steel 304L, steel (1% cr), aluminum, and copper which their thermal conductivity are 16.3, 60, 220, 304 W/m$^2$ *K, respectively.

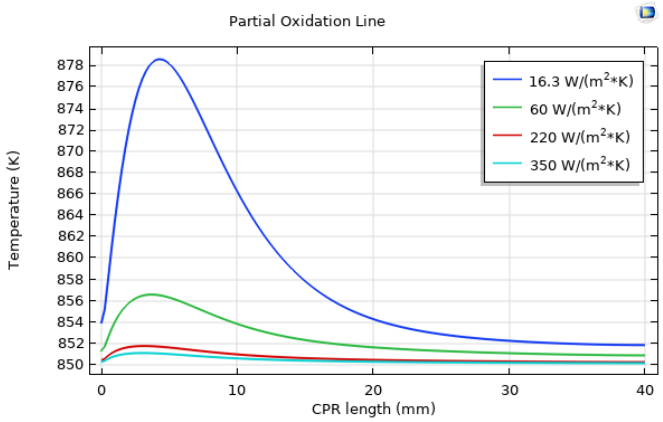


**Fig. 11.** POX/ Plate Thermal Conductivity

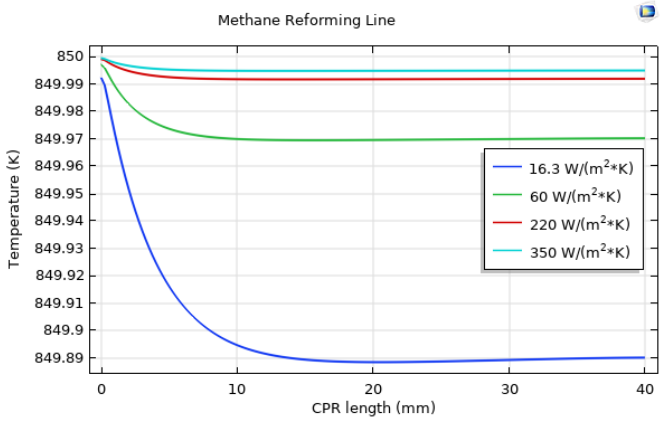


**Fig. 12.** Methane reforming/Plate Thermal Conductivity

Obviously, as the both diagrams show, there is a great jump in temperature pattern by employing steel 304L as plate material. Despite the fact that there is a tiny temperature difference in the leap of methane reforming diagram by steel 304L with inlet temperature, this difference represents itself in OPX channel with a substantial distinction around 28K. This fluctuation can damp by utilizing suitable materials like as aluminum alloys or copper with a thermal conductivity more than 220 W/m$^2$ *K.

### 5.7. Effect of Plate Length

In order to achieve the highest conversion in a CPR, it is essential to apply the appropriate plate dimensions particularly its length. Due to achieve this propose the simulation run to acquire the length that includes the highest conversion. Regarding the reforming channel as the figure 17 indicates, the trend of conversion progresses considerably before the length of 1000mm which receive to around 70% conversion. Then a modest growth is observed until the length 1200mm to the maximum conversion 75%.

In contrast, a dramatic jump at the initial length of the plate roughly shorter than 250mm is obtained in the POX channel with 90% conversion. The perfect conversion is reachable by utilizing approximately 500mm length of plate.

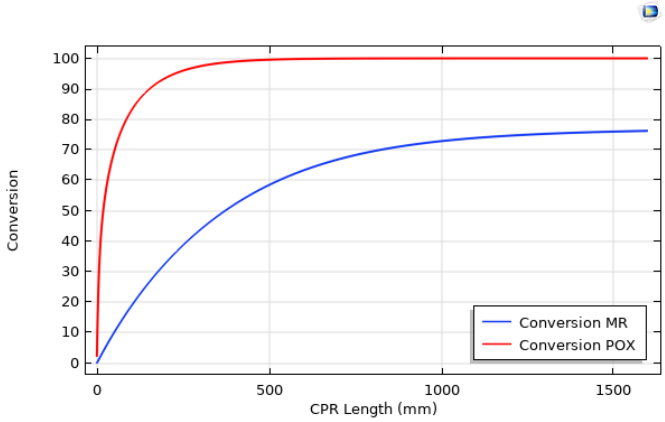


**Fig. 13.** Conversion/Plate Length

## 6. CONCLUSION

The selected 2D model provided a computational means of evaluating CR and POX coupling syngas processes in a CPR. This model covers all aspects of major chemical kinetics, heat and mass transfer phenomena in the plate type reactor. Results demonstrates that CPR combine endothermic and exothermic reactions with heat exchange in an intensified mode. Furthermore, temperature profiles illustrate an effective heat distribution along the plate reactor. The Effect of inlet temperature on methane conversion in both sides clearly conclude from the model outcomes that conversion rises by increasing temperature. Flow pattern has significant effect on the heat distribution and consequently over the counter-current configuration conversion peaks up considerably in comparison of co-current configuration. To achieve suitable rate of products according to our purpose, it is important which consider applicable feed ratio. Hence, three various proportion of products modeled in this simulation for both CR and POX sides. Although due to instant character of partial oxidation reaction the feed velocity in the POX side has a slight effect on conversion, it impacts substantially on conversion on the endothermic side. The metallic plate that has high thermal conductivity creates feasible heat transfer between endothermic and exothermic channels for small temperature differences. Additionally, to obtain the most conversion the proper plate length should be applied that it concludes in both CR and POX sides by the length 1200mm.

## 7. SYMBOLS USED

$C_p$ Heat capacity, J/kg*K
$D_{eff}$ Effective diffusion coefficient, $m^2/s$
$D_G$ Molecular diffusion coefficient, $m^2/s$
$D_k$ Knudsen diffusion coefficient, $m^2/s$
$k$ Gas thermal conductivity, $Wm^{-1}K^{-1}$ or reaction rate constant
$K_e$ Equilibrium constant
$L$ Reactor length, m
$M$ Molecular weight, kg/mol
$P_i$ Partial Pressure, bar
$r$ Reaction rate, mol/$kg_{cat}{}^3$s
$R$ Half distance between the reactor plates, m
$R_p$ Catalyst pore radius, m
$T$ Temperature, K
$u_z$ Axial mass velocity, m/s
$v$ Atomic diffusion volume
$x$ Radial coordinate, m
$X$ Conversion
$z$ Axial coordinate, m

Greek Letters

$\Delta H$ Heat of reaction, J/mol
δ Solid wall thickness, mm catalyst porosity
$\varepsilon$ Catalyst porosity
λ Thermal conductivity of solid wall, W/m*K
ϑ Stoichiometric coefficient
ρ Density, $kg/m^3$
τ Catalyst tortuosity
$\pi$ Total pressure
ω Mass fraction

Subscripts

$i$ Chemical species
$j$ Channel
n Component in excess
$r$ Reaction
$s$ Solid wall
$j = 1$ Endothermic channel (Reforming)
$i$ $= CH_4, CO, H_2, CO_2, H_2O$
n $= H_2O$
$r = 1$ Reaction (1)
$r = 2$ Reaction (2)
$r = 3$ Reaction (3)
$j = 2$ Exothermic channel (Partial Oxidation)
$i$ $= CH_4, O_2, CO, H_2, H_2O$
n $= CH_4$
$r = 1$ Reaction (13)
$r = 2$ Reaction (14)
$r = 3$ Reaction (15)

Abbreviations

ATR Autothermal Reforming
CR Steam and Dry (Couple) Reforming or combined or mixed reforming
CPR Catalytic Plate Reactor
DR Dry Reforming
FEM Finite element method
POX Partial Oxidation
SR Steam Reforming

## 8. REFERENCES


[1] Heriyanto, Heri, et al. "Syngas Production by the Gasification of Bayah's Coal over Ca (OH) 2 and Na2CO3 catalyst." World Chemical Engineering Journal 4.1 (2020): 11-17.

[2] Suhendi, Endang, Julianus Marthin Dahlin, and Yahya Almundzir. "The Effect of K2CO3 and Ca (OH) 2 Catalysts on The Yield of Syngas Products and Tar Production on Tobacco Waste Gasification with Downdraft Gasifier Type." World Chemical Engineering Journal 1.5 (2017): 75-80.

[3] Kurniawan, Teguh, Nuryoto Nuryoto, and Mochamad Adha Firdaus. "Zeolite for agriculture intensification and catalyst in Agroindustry." World Chemical Engineering Journal 3.1 (2019): 13-23.

[4] A. I. Stankiewicz, *Chem. Eng. Sci.* **2001**, *56,* 359. DOI:10.1016/S0009-2509(00)00236-0

[5] J. Hunter, G. McGuire, US4214867, **1980**.

[6] C. Ramshaw, *Chem. Eng.* **1985**, *415*, 30.

[7] Z. Anxionnaz, M. Cabassud, C. Gourdon, P. Tochon, *Chem. Eng. Process.* ***2008***, 47, 2029. DOI:10.1016/j.cep.2008.06.012

[8] T. Takeguchi, S. N. Furukawa, M. Inoue, K. Eguchi, *APPL. CATAL. A-GEN.* **2003**, *240,* 223. DOI:10.1016/S0926-860X(02)00449-0

[9] X. Zhai, Y. Cheng, Z. Zhang, Y. Jin, Y. Cheng, *Int. J. Hydrogen Energy,* **2011**, *36(12)*, 7105. DOI:10.1016/j.ijhydene.2011.03.065

[10] A. Fazeli, M. Behnam, *Int. J. Hydrogen Energy,* **2010**, *35*, 9496. DOI:10.1016/j.ijhydene.2010.05.052

[11] H. Jeong, K. Ill Kimb, T. H. Kimb, C. H. Ko, H. C. Park, I. K. Songa, J Power Sources, **2006**, *159,* 1296. DOI:10.1016/j.jpowsour.2005.11.095

[12] Mukesh Doble, Anil Kumar Kruthiventi, Green Chemistry and Engineering, Catalytic Plate Reactor Chapter 6, **2007**, 105.

[13] W. S. Dong, H. S. Roh, K. W. Jun, S. E. Park, Y. S. Oh, *APPL. CATAL. A-GEN.* **2002**, *226 (1)*, 63. DOI:10.1016/S0926-860X(01)00883-3

[14] Dalin Li, Yoshinao Nakagawa, Keiichi Tomishige, *APPL. CATAL. A-GEN.* **2011**, *408*, 1-24. DOI:10.1016/j.apcata.2011.09.018

[15] F. Besenbacher, I. Chorkendorff, B. S. Clausen, B. Hammer, A. M. Molenbroek, J. K. Nørskov, I. Stensgaard, *Science*, **1998**, *279 (5358),* 1913. DOI:10.1126/science.279.5358.1913

[16] D. L. Trimm, *Catal. Today,* **1999**, *49*, 3. DOI:10.1016/S0920-5861(98)00401-5

[17] D. Pakhare, J. Spivey, *Chem. Soc. Rev.* **2014**, *43 (22)*, 7813. DOI:10.1039/C3CS60395D

[18] Mohamed A. Al-Nakoua, Muftah H. El-Naas, *Int. J. Hydrogen Energy,* **2012**, *37*, 7538. DOI:10.1016/j.ijhydene.2012.02.031

[19] J. M. Lavoie, *Front. Chem.* **2014**, *2 (81)*, 1-17. DOI:10.3389/fchem.2014.00081

[20] G. F. Froment, *J. Mol. Catal. A Chem.* **2000**, *163*, 147. DOI:10.1016/S1381-1169(00)00407-6

[21] Won-Jun Jang, et al., *Appl. Energy,* **2016,** *173*, 80. DOI:10.1016/j.apenergy.2016.04.006

[22] Nitin Kumar, et al., *APPL. CATAL. A-GEN.*, **2016**, *517*, 211. DOI:10.1016/j.apcata.2016.03.016

[23] Nitin Kumar, Maryam Shojaee, J. J. Spivey, *Curr. Opin. Chem.*, **2015**, *9*, 8. DOI:10.1016/j.coche.2015.07.003

[24] M. Li, A. C. van Veen, *APPL. CATAL. A-GEN.*, **2018**, *550*, 176. DOI:10.1016/j.apcata.2017.11.004

[25] VR Choudhary, BS Uphade, AS Mamman, Microporous Mesoporous Mater, **1998**, *23*, 61. DOI: 10.1016/S1387-1811(98)00110-3

[26] MEE Abashar, *Int. J. Hydrogen Energy,* **2004**, *29*, 799. DOI:10.1016/j.ijhydene.2003.09.010

[27] V. R. Choudhary, K. C. Mondal, *Appl. Energy,* **2006**, *83*, 1024. DOI:10.1016/j.apenergy.2005.09.008

[28] S. Ozkara Aydınoglu, *Int. J. Hydrogen Energy,* **2010**, *35*, 12821. DOI:10.1016/j.ijhydene.2010.08.134

[29] D. V. Demidov, I. V. Mishin, M. N. Mikhailov, *Int. J. Hydrogen Energy,* **2011**, *36*, 5941. DOI:10.1016/j.ijhydene.2011.02.053

[30] M. C. J. Bradford, M. A. Vannice, *Catal Rev Sci Eng.* **1999**, *41 (1)*, 1. DOI:10.1081/CR-100101948

[31] L. Pino, A. Vita, M. Laganà, V. Recupero, *Appl. Catal. B.* **2014**, *148*, 91. DOI:10.1016/j.apcatb.2013.10.043

[32] L. Pino, A. Vita, M. Laganà, V. Recupero, *Appl. Catal. B.* **2011**, *104*, 64. DOI:10.1016/j.apcatb.2011.02.027

[33] A. Al-Fatesha, S. K. Singh, G.S. Kanade, H. Atia, A. H. Fakeeha, A. A. Ibrahim, A. M. El-Toni, N. K. Labhasetwar, *Int. J. Hydrogen Energy,* **2018**, *43 (27)*, 12069. DOI:10.1016/j.ijhydene.2018.04.152

[34] T. Yabe, K. Yamada, T. Oguri, T. Higo, S. Ogo, Y. Sekine, *ACS Catalysis*, **2018**, *8 (12)*, 11470. DOI:10.1021/acscatal.8b02476
[35] P. Ren, Z. Zhao, *Catal. Commun.* **2019**, *119*, 71. DOI:10.1016/j.catcom.2018.10.024
[36] Perry, R.H., Green, D.W., Perry's Chemical Engineers' Handbook (Ed:7th), McGraw-Hill, **1997**.
[37] Jianguo Xu, Gilbert F. Froment, *A.I.Ch.E. Journal,* **1989**, *35 (1)*, 88. DOI:10.1002/aic.690350109
[38] Jianguo Xu, Gilbert F. Froment, *A.I.Ch.E. Journal*, **1989**, *35 (1)*, 97.
[39] M. Zanfir, A. Gavriilidis, *Chemical Engineering Science,* **2003**, *58 (17)*, 3947. DOI:10.1016/S0009-2509(03)00279-3
[40] M. M. Barroso Quiroga, A. E. Castro Luna, *Ind. Eng. Chem. Res.* **2007**, *46*, 5265. DOI:10.1021/ie061645w
[41] J. R. Rostrup-Nielsen, *Catal. Sci. Technol*. **1984**, *5*. DOI:10.1007/978-3-642-93247-2_1
[42] M. A. Pena, J. P. Gomez, and J. L. G. Fierro, *APPL CATAL A-GEN.* **1996**, *144 (1-2)*, 7. DOI:10.1016/0926-860X(96)00108-1
[43] P. Pantu, G.R. Gavalas., *APPL CATAL A-GEN.* **2002**, *223*, 253. DOI:10.1016/S0926-860X(01)00761-X
[44] A.T. Ashcroft, A.K. Cheetham, J.S. Foord, M.L.H. Green, C.P. Grey, A.J. Murrell, P.D.F. Vernon, *Nature,* **1990**, *344*, 319. DOI:10.1038/344319a0
[45] D. Dissanayake, M.P. Rosynek, K.C.C. Kharas, J.H. Lunsford, *J. Catal.* **1991**, *132*, 117. DOI:10.1016/0021-9517(91)90252-Y
[46] T. Hayakawa, A.G. Andersen, M. Shimizu, K. Suzuki, K. Takehira, *Catalysis letters,* **1993**, *22*, 307. DOI:10.1007/BF00807238
[47] P.M. Torniainen, X. Chu, L.D. Schmidt, *J. Catal.* **1994**, *146,* 1. DOI:10.1016/0021-9517(94)90002-7
[48] V.R. Choudhary, A.M. Rajput, B. Prabhakar, A.S. Mamman, *Fuel,* **1998,** *77*, 1803. DOI:10.1016/S0016-2361(98)00072-6
[49] A. Slagtern, U. Olsbye, *APPL CATAL A-GEN.* **1994**, *110*, 99. DOI:10.1016/0926-860X(94)80109-6
[50] V.R. Choudhary, S.D. Sansare, A.S. Mamman, *APPL CATAL A-GEN.* **1992**, *90 (1)*, L1. DOI:10.1016/0926-860X(92)80242-5
[51] Y.F. Chang, H. Heinemann, *Catal. Lett.* **1993**, *21*, 215. DOI:10.1007/BF00769473
[52] H.Y. Wang, E. Ruckenstein, *J. Catal.* **2001**, *199*, 309. DOI:10.1006/jcat.2001.3190
[53] H.Y. Wang, E. Ruckenstein, *Catal. Lett.* **2001**, *75*, 13. DOI:10.1023/A:1016719703118
[54] A. Slagtern, H.M. Swaan, U. Olsbye, I.M. Dahl, C. Mirodatos, *Catal. Today,* **1998**, *46*, 107. DOI:10.1016/S0920-5861(98)00332-0
[55] A.P.E. York, T. Xiao, M.L.H. Green, *Top. Catal.* **2003**, *22*, 345. DOI:10.1023/A:1023552709642
[56] O. V. Buyevskaya, K. Walter, D. Wolf, M. Baerns, *Catal. Lett.* **1996**, *38*, 81. DOI:10.1007/BF00806904
[57] K. H. Hofstad, J.H.B.J Hoebink, A. Holmen, G.B. Marin, *Catal. Today,* **1998**, *40*, 157. DOI:10.1016/S0920-5861(98)00004-2
[58] E. P. J. Malens, J. H. B. J. Hoebnik, G. B. Marin, *J. Catal.* **1997**, *167*, 56. DOI:10.1006/jcat.1997.1533
[59] M. Fathi, F. Monnet, Y. Schuurman, A. Holmen, C. Mirodatos, *J. Catal.* **2000**, *190,* 439. DOI:10.1006/jcat.1999.2770
[60] M. Fathi, E. Bjorgum, T. Viig, O.A. Rokstad, *Catal. Today,* **2000**, *63*, 489. DOI:10.1016/S0920-5861(00)00495-8
[61] H. C. Yao, Y. F. Yu Yao, *J. Catal.* **1984**, *86*, 254. DOI:10.1016/0021-9517(84)90371-3
[62] A. Holmgren, B. Andersson, *J. Catal.* **1998**, *178*,14. DOI:10.1006/jcat.1998.2114
[63] K. Otsuka, K. Wang, E. Sunada, I. Yamanaka, *J. Catal.* **1998**, *175*, 152. DOI:10.1006/jcat.1998.1985
[64] H. He, H. X. Dai, L. H. Ng, K. W. Wong, C. T. Au, *J. Catal.* **2002**, *206*, 1. DOI:10.1006/jcat.2001.3466
[65] K. Otsuka, Y. Wang, M. Nakamura, *APPL CATAL A-GEN.* **1999**, *183(2)*, 317. DOI:10.1016/S0926-860X(99)00070-8
[66] C. Elmasides, T. Ioannides, X. E. Verykios, *A.I.Ch.E. Journal,* **2000**, *46(6)*, 1260. DOI:10.1002/aic.690460618
[67] G. Groppi, A. Belloli, E. Tronconi, P. Forzatti, *A.I.Ch.E. Journal,* **1995**, *41(10)*, 2250. DOI:10.1002/aic.690411008
[68] J. Chen, B. Liu, X. Gao, D. Xu, *Energies,* **2018**, *11*, 2045. DOI:10.3390/en11082045
[69] D. L. Hoang, S. H. Chan, O. L. Ding, *Chem. Eng. Res. Des.* **2005**, *83 (2)*, 177. DOI:10.1205/cherd.04151
[70] M. Zanfir, A. Gavriilidis, *Chem. Eng. Res. Des.* **2004**, *82*, 252. DOI:10.1205/026387604772992846
[71] P. Lakethe, V. M. Janardhanan, *Chem. Eng. Sci.* **2014**, *110*, 13. DOI:10.1016/j.ces.2013.05.021
[72] T. Fukuda, M. R. Harada, A. Miyazawa, *Chem. Eng. Technol.* **2019**, *42 (10)*, 2127. DOI:10.1002/ceat.201900128